molecular weight, as well as the interaction parameter and homopolymer volume fraction, thus explaining the dramatic effect of block copolymers as emulsifiers for immiscible homopolymers.

In the end, our simplified model bears a striking resemblance to phenomenological descriptions of hydrocarbon–water–surfactant systems, which postulate surfactant molecule–interface interactions and include the entropy loss due to localization in the expression for the free energy.[24] However, it was not obvious a priori that polymeric systems could be described in the same way since there is considerable rearrangement of the polymer density profiles at the interface when the surfactant is added. Moreover, our model gives a specific form for the surfactant molecule–interface interaction and allows us to predict the dependence of the interfacial tension on important parameters such as the block copolymer molecular weight.

Finally, we end with an appeal for new experiments to determine the interfacial tension and microstructure of polymeric interfaces with added block copolymer surfactants. While traditional surface tension measurements leave a lot to be desired[25] and mechanical surface wave methods[26] are difficult to apply to these systems, we believe that the use of scattering techniques may have some useful potential.

Acknowledgment. We thank L. M. Marks for editing and preparing the computer programs for publication.

Supplementary Material Available: Program A to calculate asymptotic volume fractions of all components, program B to calculate interfacial density profiles (using input from program A), and a general description of both programs (14 pages). Ordering information is given on any current masthead page.

References and Notes

(1) Olabisi, O.; Robeson, L. M.; Shaw, M. T. "Polymer–Polymer Miscibility"; Academic Press: New York, 1979.
(2) Meier, D. J., Ed. "Block Copolymers: Science and Technology"; Harwood Academic Publishers: New York, 1983; MMI Press Symposium Series, Vol. 3.
(3) Ramos, A. R.; Cohen, R. E. *Polym. Eng. Sci.* **1977**, *17*, 639.
(4) Cohen, R. E.; Ramos, A. R. *Macromolecules* **1979**, *12*, 131.
(5) Watanabe, H.; Kotaka, T. *Macromolecules* **1983**, *16*, 769.
(6) Riess, G.; Kohler, J.; Tournut, C.; Banderet, A. *Makromol. Chem.* **1967**, *101*, 58.
(7) Inoue, T.; Soen, T.; Hashimoto, T.; Kawai, H. *Macromolecules* **1970**, *3*, 87.
(8) Gaillard, P.; Ossenbach-Sauter, M.; Riess, G. In "Polymer Compatibility and Incompatibility"; Solc, K., Ed.; Harwood Academic Publishers: New York, 1982; MMI Press Symposium Series, Vol. 2, p 289.
(9) Riess, G.; Nervo, J.; Rogez, D. *Polym. Eng. Sci.* **1977**, *17*, 634.
(10) Eastmond, G. C.; Phillips, D. G. *Polymer* **1979**, *20*, 1501.
(11) Chatterjee, S. K.; Riess, G. *Polym. Bull.* **1982**, *7*, 383.
(12) Annighöfer, F.; Gronski, W. *Colloid Polym. Sci.* **1983**, *261*, 15.
(13) Noolandi, J.; Hong, K. M. *Macromolecules* **1982**, *15*, 482.
(14) Hong, K. M.; Noolandi, J. *Macromolecules* **1981**, *14*, 727.
(15) Helfand, E. *J. Chem. Phys.* **1975**, *62*, 999.
(16) Hong, K. M.; Noolandi, J. *Macromolecules* **1981**, *14*, 736.
(17) Noolandi, J.; Hong, K. M. *Polym. Bull.* **1982**, *7*, 561.
(18) Meier, D. J. *J. Polym. Sci., Part C* **1969**, *26*, 81.
(19) Leibler, L. *Macromolecules* **1980**, *13*, 1602.
(20) Leibler, L. *Makromol. Chem., Rapid Commun.* **1981**, *2*, 393.
(21) Meier, D. J., unpublished work.
(22) Leibler, L. *Macromolecules* **1982**, *15*, 1283.
(23) Cahn, J. W.; Hilliard, J. E. *J. Chem. Phys.* **1958**, *28*, 258.
(24) Antoniewicz, P. R.; Rodriguez, R. *J. Colloid Interface Sci.* **1978**, *64*, 320.
(25) Wu, S. *J. Macromol. Sci., Rev. Macromol. Chem.* **1974**, *C10* (1), 1.
(26) Van den Tempel, M.; Lucassen-Reynders, E. H. *Adv. Colloid Interface Sci.* **1983**, *18*, 281.

Dynamic Motions of Rodlike Polymers in Semiconcentrated Solution: Poly(*n*-butyl isocyanate) in Carbon Tetrachloride†

David Statman and Ben Chu*

Chemistry Department, State University of New York at Stony Brook, Long Island, New York 11794. *Received June 20, 1983*

ABSTRACT: Dynamic motions of a rodlike polymer, poly(*n*-butyl isocyanate) ($M = 7.5 \times 10^4$, $M_w/M_n \lesssim 1.2$), in carbon tetrachloride were studied by quasi-elastic laser light scattering. The Edwards and Evans model predicts that, in semiconcentrated solution, the rods should exhibit two translational motions, a free translational motion and a cooperative translational motion. Both motions have been observed. However, the cooperative motions do not appear to follow the predicted behavior exactly. The rotational motions follow the Doi and Edwards model where free translational diffusion is a determining factor.

Introduction

The equation describing the Brownian motions of a rodlike particle in an infinitely dilute solution is given by[1]

$$\partial F/\partial t = \{D_{t0\parallel}(\vec{u}\cdot\vec{\nabla}_r)^2 + D_{t0\perp}[\nabla_r^2 - (\vec{u}\cdot\vec{\nabla}_r)^2] - D_{r0}\hat{I}^2\}F \quad (1)$$

where F ($=F(\vec{r},\vec{u};t)$) is the probability of finding a rod specified by a position vector $\vec{r}$ and an orientation vector $\vec{u}$ at time t, and $\hat{I}^2$ [$=-(\sin^{-1}\theta\ \partial/\partial\theta\ \sin\theta\ \partial/\partial\theta + \sin^{-2}\theta\ \partial^2/\partial\phi^2)$] is a dimensionless orbital angular momentum operator. The "free" diffusion coefficients (at infinite dilution), $D_{t0\parallel}$, $D_{t0\perp}$, and D_{r0} are given by[2]

$$D_{t0\parallel} = k_B T \ln (L/d)(2\pi\eta_s L)^{-1} \quad (2a)$$

$$D_{t0\perp} = \tfrac{1}{2}D_{t0\parallel} \quad (2b)$$

$$D_{r0} = \tfrac{3}{2}D_{t0\parallel}L^{-2} \quad (2c)$$

where L is the length of the rod, d is the diameter, η_s is the solvent viscosity, k_B is the Boltzmann constant, and T is the absolute temperature (K).

In "semidilute" solution, defined within the limits

$$L^{-3} \ll c \ll (dL^2)^{-1} \quad (3)$$

where c is the rod number concentration per unit volume. Doi and Edwards[2] have considered rod–rod encounters which affect mainly the lateral ($D_{t\perp}$) and rotational (D_r) diffusion. They constructed a model in which the rod was

† Work supported by the National Science Foundation, Polymers Program (DMR 8314193), and the U.S. Army Research Office.

0024-9297/84/2217-1537$01.50/0

confined within a tube. Translational motion along the length of the tube was free, giving

$$D_{t\parallel}(\text{semidilute}) = D_{t0\parallel} \qquad \text{(Doi–Edwards)} \tag{4}$$

Translational motion transverse to the axis of the rod, on the other hand, was severely restricted and therefore considered to be negligible; i.e.

$$D_{t\perp}(\text{semidilute}) \rightarrow 0 \tag{5}$$

Rotational motion was predicted to be determined mainly by the rotation of the confining tube itself, which was dependent on the relative displacements of the neighboring rods. The rotational diffusion coefficient was thus given by Doi and Edwards as

$$D_r \sim D_{t0\parallel}(c^2L^8)^{-1} \tag{6}$$

Experimentally, the Doi and Edwards model has been qualitatively verified, using light scattering[3] and viscometry.[4]

In spite of qualitative verification, Edwards and Evans[5] noted that there were several discrepancies concerning the motions of rods in solutions where rod–rod interactions were prevalent. They therefore suggested that the limitations of the Doi and Edwards model involved the free diffusion of the rod along the length of the tube, viz., along the length of its axis. This assumption is valid for an infinitely thin test rod. If the rod were not infinitely thin, then the motion of the rod along its axis would have to be hindered by the presence of other rods. Edwards and Evans introduced a series of gates within the tube which open and close in order to account for the finite dimension of the rod. If the gate is closed, the rod cannot pass through. It is restricted to a space within its general locality. Once the gate opens, the rod may freely diffuse along its length until it reaches another closed gate. Thus, the equation describing the motion of the rod (eq 1) must be modified to account for the added restriction of gates that open and close. Since motion transverse to the axis of the rods is essentially prohibited, eq 1 can be rewritten as[5]

$$\left\{\frac{\partial}{\partial t} - D_{t0\parallel}(\vec{u}\cdot\vec{\nabla}_r)^2 - \sum V_\alpha + D_r\hat{I}^2\right\}F = 0 \tag{7}$$

where $\sum V_\alpha$ accounts for the effects of the gates and $D_{t0\parallel}$ is still the free diffusion coefficient. Between two gates a rod may still move along its axis without restriction. From the proposed modification of the Doi and Edwards model, Edwards and Evans were able to show that in the limit of c approaching $(dL^2)^{-1}$ rods per unit volume, the translational motion of the rod would behave according to a cooperative diffusion coefficient, $D_{t\parallel}$, such that[5]

$$D_{t\parallel} = D_{t0\parallel}[1 - G(cdL^2)^{3/2}] \tag{8}$$

where G is a proportionality constant about equal to unity.

In order to study the Edwards and Evans modification of the Doi and Edwards model, a rodlike polymer, poly(n-butyl isocyanate) (PBIC), was prepared in solution (CCl_4) at concentrations approaching $c = (dL^2)^{-1}$ rods per unit volume. Quasi-elastic laser light scattering was used to observe the motions of rodlike polymers in solution.

Light Scattering

If, to a first approximation, the rotational and translational motions of the rod can be considered to be effectively decoupled (see ref 3 and 6) and if the relative motions of the rods with respect to each other can be considered to be *statistically* independent of one another, then the characteristic function of the light scattered from a solution of rodlike polymers can be given by[7]

$$I_{fi}(\vec{K},t) = A^2\{[G_1(\vec{K},t)] \times [t_{00}^{fi*}t_{00}^{fi}(\alpha_0^0)^2 + \tfrac{1}{5}(\alpha_2^0)^2 \exp[-6D_r t](\sum_{L=-2}^{2} t_{2L}^{fi*}t_{2L}^{fi})]\} \tag{9}$$

where A^2 is taken as an experimental constant, α_0^0 and α_2^0 are elements of the polarizability tensor of the scattering segment in spherical tensor notation, t is the time, $\vec{K}$ is the scattering vector, whose magnitude is given by

$$|K| = \frac{4\pi n}{\lambda_0}\sin\left(\frac{\theta}{2}\right) \tag{10}$$

θ is the scattering angle, λ_0 is the wavelength of the incident light in vacuo, n is the refractive index of the scattering medium, and t_{JL}^{fi} are the elements of the transformation matrix which takes the polarizability tensor into the scattering geometry, and f and i correspond to the final and initial directions of the electric field vector of the polarized light, respectively. $G_1(\vec{K},t)$ is given by

$$G_1(\vec{K},t) = \int d\vec{r}\,[\exp(i\vec{K}\cdot\vec{r})G_1(\vec{r}|\vec{r}_0;t)] \tag{11}$$

and $G_1(\vec{r}|\vec{r}_0;t)$ is the Greens function solution to

$$\left\{\frac{\partial}{\partial t} - D_{t0\parallel}(\vec{u}\cdot\vec{\nabla}_r)^2 - \sum V_\alpha\right\}G_1(\vec{r}|\vec{r}_0;t) = \delta(\vec{r} - \vec{r}_0)\delta(t) \tag{12}$$

where $\delta(x)$ is the Dirac δ function. $\vec{u}$, $\vec{r}$, and $\vec{r}_0$ are in the x direction, giving $\vec{u}\cdot\vec{\nabla}_r = \partial/\partial x$.

From eq 9, it can be shown that

$$I_{Vv}(\vec{K},t) = A^2\{[G_1(\vec{k},t)][\tfrac{1}{3}(\alpha_0^0)^2 + \tfrac{2}{15}(\alpha_2^0)^2 \exp[-6D_r t]]\} \tag{13a}$$

and

$$I_{Hv}(\vec{K},t) = A^2\{[G_1(\vec{K},t)][\tfrac{1}{10}(\alpha_2^0)^2 \exp[-6D_r t]]\} \tag{13b}$$

The time autocorrelation function of the scattered light is given by[8]

$$\langle I_{fi}(\vec{K},t)I_{fi}(\vec{K},0)\rangle = [I_{fi}(\vec{K},0)]^2 + [I_{fi}(\vec{K},t)]^2 \tag{14}$$

Therefore, the square root of the time autocorrelation function of the intensity of light scattered from a solution of rodlike polymers (where the base line, given by $[I_{fi}(\vec{K},0)]^2$, has already been subtracted) will give the characteristic function in eq 9.

In eq 13a and 13b, the quantity of interest is $G_1(\vec{K},t)$. In order to find $G_1(\vec{K},t)$, eq 11 must be solved. Edwards and Evans[5] pointed toward the solution for $G_1(\vec{K},t)$. Equation 12 may be rewritten as

$$\left\{\frac{\partial}{\partial t} - D_{t0\parallel}\frac{\partial^2}{\partial x^2} - \sum V_\alpha\right\}G_1(x|x_0;t) = \delta(x - x_0)\delta(t) \tag{12a}$$

the solution to which is[6]

$$G_1(x|x_0;t) = G_0(x|x_0;t) + \rho_B\int\frac{dK}{2\pi}\{\exp[-iK(x - x_0)] \times \exp(-2D_{t\parallel}K^2t)(\text{constant factor} + \ldots)\} \tag{15}$$

where $G_0(x|x_0;t)$ is the solution to

$$\left\{\frac{\partial}{\partial t} - D_{t0\parallel}\frac{\partial^2}{\partial x^2}\right\}G_0 = \delta(x - x_0)\delta(t) \tag{16}$$

ρ_B is the number of gates that the test rod encounters per unit length per unit time,[5] $D_{t\parallel}$ is given by eq 8, and the constant factor is a function of the scattering angle as well as other parameters. From eq 15, $G_1(\vec{K},t)$ can be written as

$$G_1(\vec{K},t) = \exp[-K^2D_{t0\|}t] + \exp[-2K^2D_{t\|}t](\text{constant factor} + ...) \quad (17)$$

where ρ_B has now been absorbed by the constant factor. By combining eq 17 with eq 9, we finally obtain for the characteristic function

$$I_{fi}(\vec{K},t) = A^2\{\exp[-K^2D_{t0\|}t] + B\exp[-2K^2D_{t\|}t]\}\{C + D\exp[-6D_rt]\} \quad (18)$$

where C and D depend on f and i, as per eq 13a and 13b.

From eq 18, it can be seen that the scattered light is dependent on the rotational motion as well as both the "free" translational motion between two gates and the cooperative translational motion as determined by the opening and closing of these gates. The free translational diffusion coefficient $D_{t0\|}$ is represented by eq 2a and the cooperative translational diffusion coefficient $D_{t\|}$ obeys eq 8. The rotational diffusion coefficient should be given by eq 6, although it is not clear whether or not $D_{t0\|}$ should be replaced by $D_{t\|}$.

Selection of a Rodlike Polymer System

There are many examples of particles that have rodlike structures. These could include short strands of DNA, α-helical polypeptides,[8] thin[9] and thick[10] muscle filaments, xanthan polysaccharides,[11] PBLG,[12] and some synthetic polymers.[13-16] It is desired, for the present study, that the rods chosen for examination be as simple as possible. The requirements imposed are rigidity, minimal ionic interactions, and uniformity in the polarizability tensor along the length of the rod. Most biological and natural structures that are rigid account for their rigidity through charge interactions. Some rodlike polymers, such as poly(1,4-phenylterephthalamide) (PPTA) and poly(benzobisoxazole) (PBO) require solvents that can protonate the polymers. Therefore, we need to study the aggregation and charge interactions as a function of ionic strength of the solution. In the polyisocyanate family, for instance, poly(*n*-butyl isocyanate), poly(*n*-hexyl isocyanate), and poly(*n*-octyl isocyanate) are known to be rigid.[17] Poly(*n*-butyl isocyanate) (PBIC) stands out as being more rigid than the others.[18,19] The primary structure of PBIC is

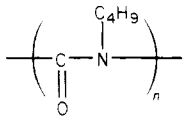

where n is the number of monomer units in the polymer. PBIC is an R-1 nylon. The secondary structure is helical with an axial rise of 0.16 nm per monomer unit (–C(O)N-(C_4H_9)–).[18] This means that PBIC has a structure similar to that of α-helical polypeptides, which, in general, have an axial rise of 0.15 nm per monomer.[20] The tertiary structure of PBIC is a relatively rigid rod, when the length is less than about 160 nm.[17-20] The length of the rod is related to the molecular weight by 99 daltons per 0.16 nm. A polymer with a molecular mass greater than 9×10^4 daltons, therefore, is no longer a rigid rod but instead a stiff worm.[18,20] The diameter of the rod is about 1.5 nm.[18,20]

The intrinsic viscosity of PBIC for molecular masses under 150 000 daltons was found to follow the relationship known for rods[18] with

$$[\eta] = AM^2 \quad (19)$$

where $A = 7.6 \times 10^{-10}$ dL/(g (dalton)^2) for PBIC, $[\eta]$ is in dL g^{-1}, and M is in daltons. Theory[21] shows that while for random coils the exponent to the molecular weight approaches 0.5, as the polymer becomes rigid, this exponent increases to values between 1.85 and 2. Intrinsic viscosity measurements have indicated that the rigidity of PBIC is solvent dependent. PBIC is most rigid in carbon tetrachloride.[19] To confirm this, the persistence length of the polymer was measured in different solvents[18,20,22] and was found to vary from 60 nm in chloroform to 160 nm in carbon tetrachloride.

PBIC is not without problems. The polymer does not have a high solubility in anything.[17] When attempts were made to form liquid crystals at concentrations the order of $8(dL^2)^{-1}$, as predicted by Flory, the polymer formed solid crystals.[17] Fortunately, this crystallization did not present too much of a problem in the range of concentrations applicable to the present study. Preparation of semiconcentrate solutions, however, was not a trivial problem. In addition, the polarizability tensor of a scattering segment of PBIC is very close to most solvents that it will dissolve in. In fact, $(\partial n/\partial c)$, which is related to the polarizability tensor, is about 0.06 cm^3 g^{-1} in chloroform.[22] Thus, light scattering measurements in dilute and semidilute solutions have relatively low signal-to-noise ratios. We have to limit this study to the semiconcentrate solution where the scattered intensity is reasonable.

Experimental Methods

A. Preparation of Poly(*n*-butyl isocyanate) (PBIC). PBIC samples were prepared following a method similar to the one used by Aharoni.[17] Modification of the procedure by Shashoua, Sweeney, and Tietz[23] can be found elsewhere (see ref 6). The polymer was fractionated into different molecular weight fractions using CCl_4 as the good solvent and methanol as the poor solvent. For all measurements, CCl_4 was the solvent used. The molecular weight was determined by measuring the intrinsic viscosity of the polymer.

The refractive index increment, $\partial n/\partial c$, at different wavelengths was measured in a Brice-Phoenix differential refractometer at 30 °C. $\partial n/\partial c$ at $\lambda_0 = 488$ nm was interpolated from these measurements to be $0.040 \pm 5\%$ cm^3 g^{-1}. This value is consistent with the measurements reported by Fetters and Yu.[22]

We were particularly concerned with the aggregation problem. In fact, the selection of the PBIC/CCl_4 system was partially based on this consideration. Apparently, Ambler et al.[19] Burr and Roberts,[20] Fetters and Yu,[22] and Aharoni[17] were able to prepare solutions of PBIC without severe aggregation problems. Nevertheless, we tried to make independent tests to ensure a lack of aggregation in our PBIC solutions. For PBIC in CCl_4, the low refractive index increment ($\sim$0.04 cm^3 g^{-1}) and low molecular weight of our PBIC sample prevented us from measuring (with precision) the angular distribution of absolute scattered intensity in dilute solutions. Thus, we were not able to make an absolute and independent calibration of the molecular weight of our fractionated PBIC sample. However, we did use three separate criteria to justify indirectly that our solution preparations have negligible aggregation. One of the three criteria is to use the viscosity plots as follows.

In dilute solutions, the concentration-dependent viscosity should follow both the Huggins relation

$$\eta_{sp}/c = [\eta] + K'[\eta]^2c \quad (20)$$

and the Kraemer relation

$$(\ln \eta_{rel})/c = [\eta] - K''[\eta]^2c \quad (21)$$

where η_{sp} is the specific viscosity given by $(\eta - \eta_s)/\eta_s$, η_{rel} is the relative viscosity given by η/η_s, and η_s is the viscosity of the solvent in centipoise. K' is the Huggins constant and K'' is the Kraemer constant. Figure 1 shows the concentration dependence of both η_{sp}/c and $(\ln \eta_{rel})/c$. $[\eta] = 4.40$ dL g^{-1}, corresponding to a molecular mass of 7.5×10^4 daltons. K' was calculated, using a linear least-squares line fit routine, to be 0.44, which is consistent with the value reported by Ambler et al.[19]

From eq 19, the molecular mass of the sample was determined to be 7.5×10^4 daltons. A 7.5×10^4 dalton polymer is (7.5×10^4

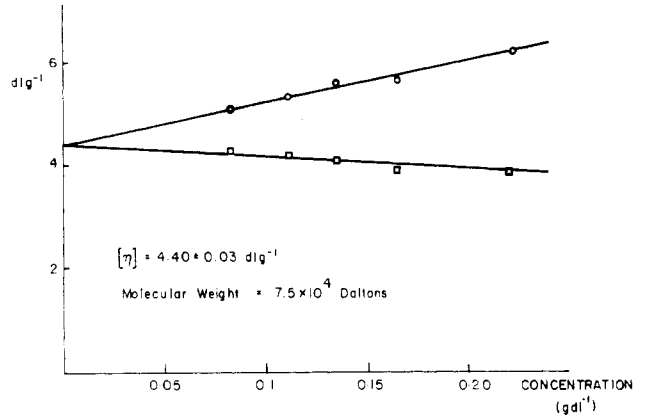

Figure 1. Plots of η_{sp}/c (hollow circles) and ln $(\eta_{rel})/c$ (hollow squares) as a function of concentration. The upper curve obeys Huggins' relation, eq 20, with $K' = 0.44 \pm 0.03$ and the lower curve obeys the Kraemer relation, eq 21. $[\eta] = 4.40 \pm 0.03$ dL g^{-1}, corresponding to a polymer molecular weight of 7.5×10^4.

daltons × (0.16/99) nm/dalton) = 120 nm long. In CCl_4 the persistence length, $(2\gamma)^{-1}$, is 160 nm.[18-20] $2\gamma L = 0.75$. The sample can be considered as rods. The axial ratio for a single rod is 80. Therefore, $c^* \approx (dL^2)^{-1} \approx 0.01$ g cm^{-3}. Since c^* is inversely proportional to the molecular weight of the rod, polydispersity should not have a pronounced effect on the experimental results as long as the molecular weight distribution is not broad. For instance, in the present case, as will be shown later, $M_w/M_n \leq 1.2$. This means that, assuming a Schultz distribution with cutoffs at a distribution height of $^1/_3$, $0.005 \leq c^* \leq 0.012$ g cm^{-3}. Nevertheless, the properties being studied do not preclude a distribution of molecular weight. Therefore, the quantities measured, especially near c^*, will be considered to be average values over a relatively narrow molecular weight distribution.

B. Laser Light Scattering. For PBIC, I_{Hv} is very small. In fact, the ratio of I_{Hv} to I_{Vv} at 30 °C is on the order of 3% as measured. Thus, $I_{Vv}(\vec{K},t)$ contains basically only those components involving translational motion, while $I_{Hv}(\vec{K},t)$ will contain the components involving both translational and rotational motions.

Figure 2 shows a block diagram of the experimental setup, which has been described elsewhere.[24] The laser was an argon ion laser (Lexel Model 92) tuned at 488-nm wavelength. The temperature was maintained at 30.00 ± 0.05 °C. The output signal of the photomultiplier was sent through an SSR preamplifier and discriminator (Model 1106) and then to a Malvern Scientific digital autocorrelator (Model K7023) which calculated the time correlation function of the scattered intensity. The laser power was maintained at 250 mW for all measurements.

Light scattering demands that all samples be essentially free of dust. Generally, a dust-free solution is prepared by filtration. Unfortunately, PBIC is often filtered out easily along with the dust. Therefore, a different method was developed. PBIC was dissolved in filtered CCl_4 and the stock solution was centrifuged in a Sorvall (RC2-B) centrifuge at $7.7 \times 10^3 g$. The middle fraction was taken, and aliquots were put in optical cells and diluted to the desired concentrations with filtered CCl_4. All preparations were done in a glovebox filled with dried and filtered N_2 gas. Since the density of dust is generally *less* than the density of CCl_4, this method was not as effective as might have been preferred.

On the basis of eq 14

$$G^{(2)}(K,t) = \langle I_{fi}(\vec{K},t) I_{fi}(\vec{K},0)\rangle = A(1 + b|g^{(1)}(K,t)|^2) = [I_{fi}(\vec{K},0)]^2 + [I_{fi}(\vec{K},t)]^2$$

the unnormalized electric field time correlation function has the form

$$b^{1/2} g^{(1)}(K,t) = I_{fi}(\vec{K},t)/I_{fi}(\vec{K},0) = b^{1/2} e^{-\Gamma t} \quad (22)$$

where we have taken b to be an adjustable parameter in the data fitting procedure. For a polydisperse sample

$$g^{(1)}(\tau) = \int_0^\infty G(\Gamma) e^{-\Gamma\tau}\, d\Gamma \quad (23)$$

where $G(\Gamma)$ is the normalized characteristic line width distribution

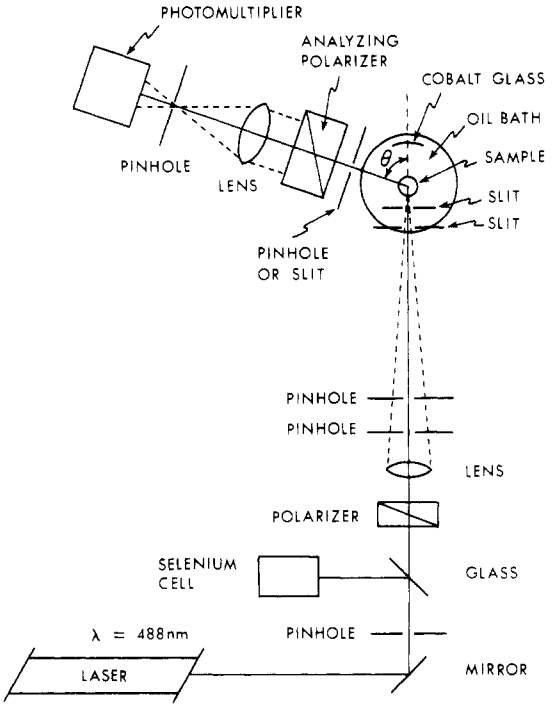

Figure 2. Experimental setup for light scattering measurements as described in the text.

function. In our analysis, we used both the cumulants method[24] and the double-exponential fit. In the cumulants method, we can determine the average line width $\bar{\Gamma}$ and the variance $\mu_2/\bar{\Gamma}^2$ whenever the magnitude of $\mu_2/\bar{\Gamma}^2$ is not too large (≤0.3):

$$\bar{\Gamma} = \int_0^\infty G(\Gamma)\Gamma\, d\Gamma \quad (24)$$

$$\mu_2 = \int_0^\infty G(\Gamma)(\Gamma - \bar{\Gamma})^2\, d\Gamma \quad (25)$$

by fitting the net photoelectron count single-clipped time correlation function to

$$\ln (Ab)^{1/2}|g^{(1)}(t)| = \ln (Ab)^{1/2} - \bar{\Gamma}t + {}^1/_2(\mu_2/\bar{\Gamma}^2)(\bar{\Gamma}t)^2 + B_3(\bar{\Gamma}t)^3 \quad (26)$$

The last term, $B_3(\bar{\Gamma}t)^3$, represents expansion to third order. When the characteristic decay times are far apart, we can approximate the time correlation function using a double-exponential fit:

$$(Ab)^{1/2} g^{(1)}(t) = A_1 \exp(-\Gamma_1 t) + A_2 \exp(-\Gamma_2 t) \quad (27)$$

where A_1 and A_2 are the two amplitude factors associated with Γ_1 and Γ_2. For rodlike polymers, eq 18 has the same form as eq 27. However, eq 18 and 27 represent the dynamical behavior of a monodisperse rodlike polymer. In our case, our PBIC polymer has a finite size distribution.

According to eq 2a, we have

$$D_{t0\|} \propto (\ln M)/M \quad (28)$$

since $L \propto M$. For usual molecular weight distributions, we can write $D_{t0\|} \propto 1/M$ and in the limit of infinite dilution and zero scattering angle, we can then derive[12]

$$M_w/M_n = 1 + \mu_2/\bar{\Gamma}^2 \quad (29)$$

From the cumulants analysis on time correlation function measurements from dilute solutions of PBIC in CCl_4 (and in chloroform), we obtained $M_w/M_n < 1.2$, signifying that our fractionated PBIC polymer sample has a fairly narrow molecular weight distribution. We have used this low M_w/M_n value as well as Figure 1 to imply that aggregation is not a problem for PBIC in dilute solutions of CCl_4. If aggregation is serious, the variance $\mu_2/\bar{\Gamma}^2$ is very sensitive to the presence of a substantially different (low) characteristic line width.

As the new line width distribution $G^*(\Gamma) = G_p(\Gamma) + G_a(\Gamma)$, with $G_a(\Gamma)$ being the additional characteristic line width distribution

Table I
Correlation Length and Osmotic Compressibility of PBIC (7.5×10^4 daltons) in CCl_4 at Different Concentrations

c, g cm^{-3}	$10^6(\partial\pi/\partial c)/RT$,[a] mol g^{-1}	ξ, nm	$10^{17}\xi^2(\partial\pi/\partial c)/RT$, mol cm^2 g^{-1}
0.0031	1.60	36	2.1
0.0055	0.86	42	1.5
0.0096	0.37	67	1.7
0.014	0.40	62	1.6
0.015	0.65	49	1.5

[a] ±10%.

due to aggregates, the average line width in the presence of aggregation has the form

$$\bar{\Gamma}^* = \int G^*(\Gamma)\Gamma\, d\Gamma = A_p\bar{\Gamma} + A_a\bar{\Gamma}_a \quad (30)$$

where A_p ($=\int G_p(\Gamma)\, d\Gamma$) and A_a ($=\int G_a(\Gamma)\, d\Gamma$) are the normalization factors for $G_p(\Gamma)$ and $G_a(\Gamma)$ with $A_p + A_a = 1$ and are related to the relative intensity of light scattered by the polymer PBIC and its aggregates (if any), respectively. By substituting eq 30 into eq 25, we get

$$\mu_2^* = A_pA_a(\bar{\Gamma} - \bar{\Gamma}_a)^2 + A_p\mu_2 + A_a\mu_{2,a} \quad (31)$$

where

$$\mu_{2,a} = \int G_a(\Gamma)(\Gamma - \bar{\Gamma}_a)^2\, d\Gamma/A_a \quad (32)$$

and

$$\mu_2 = \int G_p(\Gamma)(\Gamma - \bar{\Gamma})^2\, d\Gamma/A_p \quad (33)$$

are the second moments of the polymer and its aggregates (if any). The main contribution for a larger μ_2^* comes from the square of the difference in line widths $(\bar{\Gamma} - \bar{\Gamma}_a)^2$.

At higher concentrations, since we are investigating a new characteristic time, we can no longer use the variance agreement to imply lack of aggregation. So, we have measured the angular distribution of scattered intensity as a function of time. Many PBIC solutions were checked twice daily over a period of 4 weeks and no increase in scattered intensity at small scattering angles was observed.

The method of analysis for the angular distribution of integrated scattered intensity was based on the relation

$$R_{Vv}(0)/R_{Vv}(K) \approx 1 + \xi^2K^2 \quad (34)$$

where ξ is a correlation length and $R_{Vv}(K)$ is the excess Rayleigh ratio due to concentration fluctuations at K. At $K = 0$

$$R_{Vv}(0) = HCRT/(\partial\pi/\partial c)_{T,P} \quad (35)$$

where H is the optical constant and $(\partial\pi/\partial c)_{T,P}$ is the osmotic compressibility. Table I shows some typical correlation lengths and osmotic compressibilities for PBIC (molecular mass 7.5×10^4 daltons) in CCl_4 at different concentrations. The correlation length (with large uncertainties) shows only small variations in this concentration range. We have also noted an empirical relation indicating $\xi^2(\partial\pi/\partial c)/RT$ to be relatively constant. In any case, the concentration behavior of ξ and $(\partial\pi/\partial c)_{T,P}$ also suggests lack of aggregation.

Results and Discussion of Dynamic Data

Figures 3a, 4a, and 5a are examples of measured time correlation functions at 0.0082 g/cm^3. Each correlation function has 92 points that span 2–3 characteristic decay time periods. In each figure, the net photoelectron count single-clipped time correlation function is plotted, as well as the negative of the logarithm of the correlation function, against time. The base lines of the correlation functions, corresponding to $[I_{fi}(K,0)]^2$ in eq 14, were subtracted. According to eq 13a and 17, $I_{Vv}(K,t)$ is expected to be a double exponential, with the decay times of the two exponentials being orders of magnitude apart. It was necessary to use different delay times, $\delta\tau$, between channels

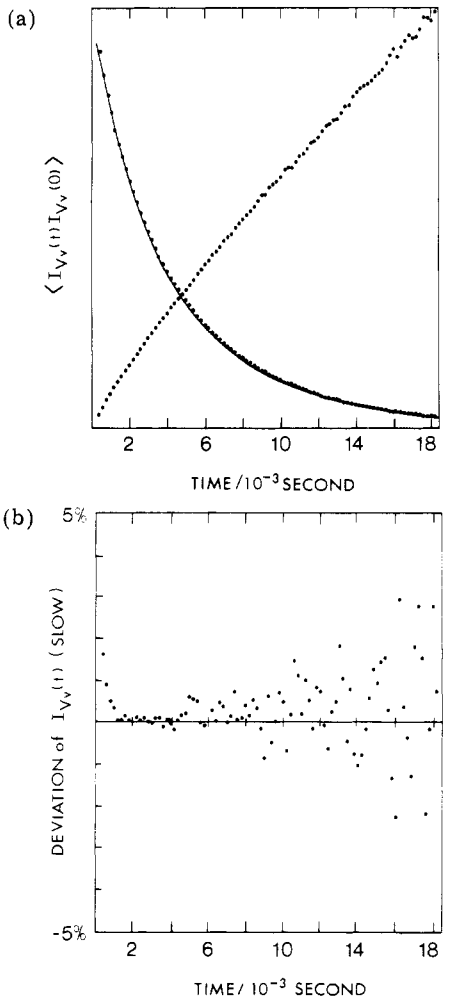

Figure 3. (a) Normalized slow decay time correlation function of $I_{Vv}(K,t)$ with the base line subtracted and negative logarithm of that correlation function. Concentration = 0.0082 g cm^{-3}. Scattering angle, θ, = 60°. The measured correlation function is fitted to a double exponential given by $A_1 \exp(-t/\tau_1) + A_2 \exp(-t/\tau_2)$ with $A_1 + A_2 = 1$. The calculated curve is represented by the solid line with $A_1 = 0.826$, $A_2 = 0.174$, $\tau_1 = 12.2 \times 10^{-3}$ s, $\tau_2 = 3.89 \times 10^{-3}$ s, $\bar{\tau}_{Vv}$(slow) ($\equiv A_1\tau_1 + A_2\tau_2$) $= 7.76 \times 10^{-3}$ s. The double exponential is used to approximate the line width distribution. Individual values of A_1, A_2, τ_1, and τ_2 are representative components modeling the line width distribution. Therefore, only $\bar{\tau}_{Vv}$(slow) and $(\mu_2/\bar{\Gamma}^2)_{slow}$ have physical meaning. (b) Plot of the deviation of the measured correlation function of (a), from the calculated fit (see caption to (a)). DEV = (measured − fit)/measured.

in measuring the correlation function if we were to observe both characteristic decay times. Figure 3a shows a correlation function with a decay due to the cooperative motions of the rods. From the logarithm plot, we can see that the time correlation function does not have a single-exponential decay; instead it has a continuous distribution of exponentials which is not too broad. This characteristic line width distribution has two sources: (a) polydispersity and (b) interparticle interactions. It is not clear from Figure 3a that there is a fast component corresponding to the free translational motion of the rod within a tube as predicted by eq 18. In order to determine whether or not such a fast component exists, the delay time increment was shortened significantly when compared with the delay time range in Figure 3a. Figure 4a shows the time correlation function for the same sample as in Figure 3a, with the delay time increment being about 2 orders of magnitude less than that for Figure 3a. From the logarithm plot in Figure 4a, we can see that a fast characteristic decay time

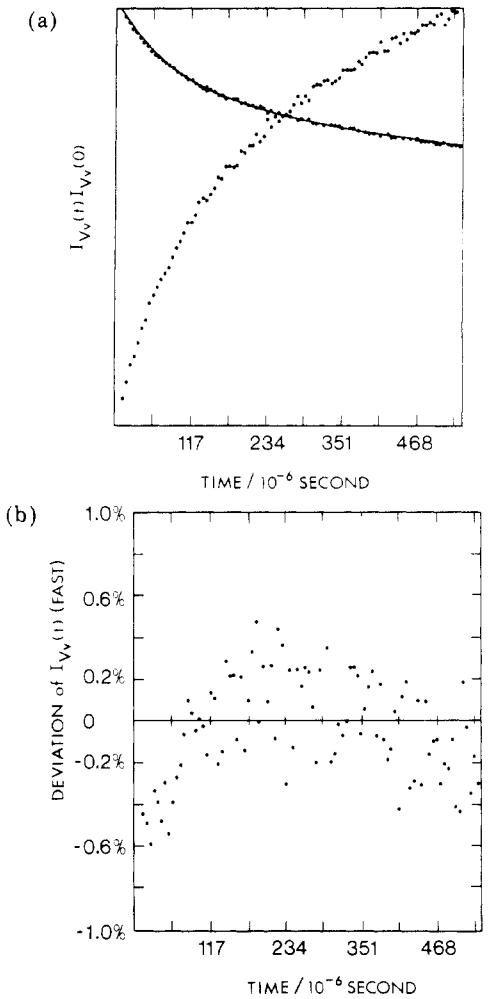

Figure 4. (a) Normalized fast decay time correlation function of $I_{Vv}(K,t)$ with the base line subtracted and the negative logarithm of that correlation function. Concentration = 0.0082 g cm^{-3}. Scattering angle, θ, = 60°. The correlation function is fitted as described in the text. The characteristic time, $\bar{\tau}_{Vv}$(fast) for the fast decay in the figure is $\bar{\tau}_{Vv}$(fast) = 10.4 × 10^{-5} s. The solid line is the calculated fit given by $\{B_1[A_1 \exp[-t/\tau_1] + A_2 \exp[-t/\tau_2]] + B_2 \exp[-t/\bar{\tau}_{Vv}(\text{fast}) + [\mu_2\bar{\tau}_{Vv}(\text{fast})(t/\bar{\tau}_{Vv}(\text{fast}))^2/2]$, where $\mu_2\bar{\tau}_{Vv}^2$(fast) = 0.18, A_1, A_2, τ_1 and τ_2 are given in Figure 3a, and B_1 and B_2 are proportionality constants. (b) Plot of the deviation of the measured correlation function of (a), from the calculated fit shown in Figure 3a, normalized to the measured value. DEV = (measured − fit)/measured.

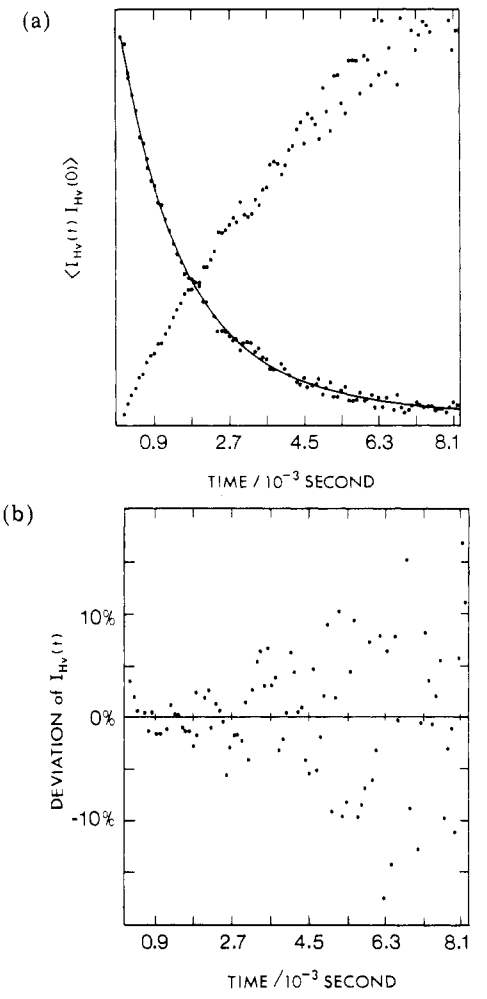

Figure 5. (a) Normalized time correlation function of $I_{Hv}(K,t)$ with the base line subtracted and negative logarithm of that correlation function. Concentration = 0.0082 g cm^{-3}. Scattering angle, θ, = 60°. The measured correlation function is fitted to a double exponential given by $A_1 \exp(-t/\tau_1) + A_2 \exp(-t/\tau_2)$ with $A_1 + A_2 = 1$. The calculated curve is represented by the solid line with A_1 = 0.273, A_2 = 0.727, τ_1 = 19.2 × 10^{-3} s, τ_2 = 2.69 × 10^{-3} s, and $\bar{\tau}_{Hv}$ ($\equiv A_1\tau_1 + A_2\tau_2$) = 3.52 × 10^{-3} s. Again, τ_1 and τ_2 have no physical meaning. (b) Plot of the deviation of the measured correlation function of (a) from the calculated fit shown in (a), normalized to the measured value. DEV = (measured − fit)/measured.

does exist. This fast characteristic line width is due to the free diffusion coefficient within the Edwards tube. The time correlation function spanning over the long decay time range, as shown in Figure 3a, is not affected by the fast characteristic decay time (due to free diffusion) since the fast component decays rather rapidly over a relatively short delay time range. Therefore, the slow decay time correlation function can be analyzed independent of the fast decay time correlation function. This was done by taking the square root of the slow decay time correlation function and fitting it to a double-exponential form. In this case, the double-exponential fit has no physical meaning. It is being used as a model to compute the average decay time, $\bar{\tau}$. Accordingly, based on eq 27, $\bar{\tau}_{Vv}$(slow) [$\equiv(A_1\tau_1 + A_2\tau_2)/(A_1 + A_2)$] was determined by weighting each of the two apparent decay times determined from the double-exponential fit by its preexponential factor and taking the weighted average of these two apparent decay times. The solid line in Figure 3a is the computed apparent double-exponential curve. It should be noted that A_1 and A_2 have the form of eq 27 but are not amplitude factors related to two distinct apparent characteristic line widths Γ_1 and Γ_2.

The fast decay time correlation function (Figure 4a) is determined primarily by free diffusion. However, the shape of the curve is modulated by the slow correlation function. Therefore, as can be seen from eq 18, a linear extrapolation to the initial decay will not necessarily give the proper fast decay time. The slow decay correlation function should be subtracted in order to do the analysis properly. Double-exponential fitting did not provide a reasonable analysis, as it does not give values for τ_{Vv}(slow) that agree with the calculated slow decay time correlation functions. This can be attributed, in part, to the fact that each of the two characteristic decays is actually a distribution of decays, corresponding to a bimodal line width distribution. Although each peak of the bimodal line width distribution can be represented by an apparent double-exponential fit, the correlation function at short delay times contains contributions from both fast and slow characteristic times. In order to properly subtract the slow decay contribution in the fast decay time correlation function, the coefficients (B_1 and B_2 as stated in Figure

4a) were varied until the result could be fitted to a second-order cumulants[25]

$$(A\beta)^{1/2}g^{(1)}(t) = B_1[A_1 \exp(-t/\tau_1) + A_2 \exp(-t/\tau_2)] + B_2 \exp[-t/\bar{\tau}_{Vv}(\text{fast}) + \mu_2\bar{\tau}_{Vv}(\text{fast})(t/\tau_{Vv}(\text{fast}))^2/2] \quad (36)$$

to give the fast decay time. The values of A_1, A_2, τ_1, and τ_2 were obtained from the slow characteristic decay time studies, while B_1 and B_2 are the amplitude factors related to the slow and fast characteristic frequency distribution functions, respectively. The $\mu_2\bar{\tau}^2$ variance term in the second-order cumulants fit for the fast decay time was the same as that when the slow decay time correlation function was fitted to a second-order cumulants. It should be noted that if the calculated fast decay exponential were subtracted from the slow decay time correlation function, we would obtain the same result for the slow characteristic time. The calculated time correlation function for Figure 4a used the results from the second-order cumulants fit on the fast time correlation function and an apparent double-exponential fit on the slow time correlation function. The two results were multiplied by the appropriate coefficients (B_1 and B_2) determined by the above procedure and were added together to give a total time correlation function. This is represented by the solid line in Figure 4a. Figures 3b and 4b show the deviations of the measured time correlation functions from the calculated correlation functions in order to indicate the "goodness" of the fit. Figure 5a shows a plot of the time correlation function $\langle I_{Hv}(K,t)I_{Hv}(K,0)\rangle$. The square root of $\langle I_{Hv}(K,t)I_{Hv}(K,0)\rangle$ was fitted to a double-exponential form. The average decay was determined by using the weighted average in the same manner as for the slow decay time correlation function described above. The solid line in Figure 5a is the calculated time correlation function. Figure 5b shows the deviation of the measured correlation function from the calculated correlation function in order to indicate the "goodness" of the fit. Parts a–c of Figure 6 show plots of the inverse of the average decay time $\bar{\tau}$ against both $\sin^2(\theta/2)$ and K^2 (the square of the scattering vector, given by $16\pi^2n^2/\lambda_0^2 \sin^2(\theta/2)$) for the time correlation functions of $I_{Vv}(\text{fast})$, $I_{Vv}(\text{slow})$, and I_{Hv}, respectively. The slopes and intercepts of $\bar{\tau}^{-1}$ vs. K^2 were calculated with a linear least-squares routine. The slope of $\bar{\tau}^{-1}$ for $\langle I_{Hv}(K,t)I_{Hv}(K,0)\rangle$ vs. K^2 is within 5% of the slope of $\tau^{-1}(\text{slow})$ for $\langle I_{Vv}(K,t)I_{Vv}(K,0)\rangle$ vs. K^2 for each concentration. The cooperative diffusion coefficient is given by

$$D_{t\parallel} = \tfrac{1}{2}(\text{slope})(\bar{\tau}_{Vv}^{-1}(\text{slow}) \text{ vs. } K^2) = \tfrac{1}{2}(\text{slope})(\bar{\tau}_{Hv}^{-1} \text{ vs. } K^2) \quad (37)$$

The free diffusion coefficient is given by

$$D_{t0\parallel} = (\text{slope})(\bar{\tau}_{Vv}^{-1}(\text{fast}) \text{ vs. } K^2) \quad (38)$$

The rotational diffusion coefficient is given by

$$D_r = \tfrac{1}{6}(\text{intercept})(\bar{\tau}^{-1} \text{ vs. } K^2) \quad (39)$$

Equations 37, 38, and 39 come directly from eq 18.

The first important result is that $D_{t0\parallel} = 2.8 \times 10^{-7}$ cm^2 s^{-1} $\approx 10^{-7}$ cm^2 s^{-1} as calculated by eq 38 and the decomposition of exponentials described above and *appears* to be independent of concentration, which is another indication that aggregation is not likely to be an important effect in this concentration range, as shown in Figure 6a. The measured value of $D_{t0\parallel}$ is consistent with eq 2a, which gives an ideal value for $D_{t0\parallel}$ on the order of 10^{-7} cm^2 s^{-1}. This agreement suggests that within the Edwards tube, the diffusion of the rod along its axis is *essentially* free as we have computed according to eq 2a.

The cooperative diffusion coefficient, characteristic of translational motions, has been observed via the slow decay

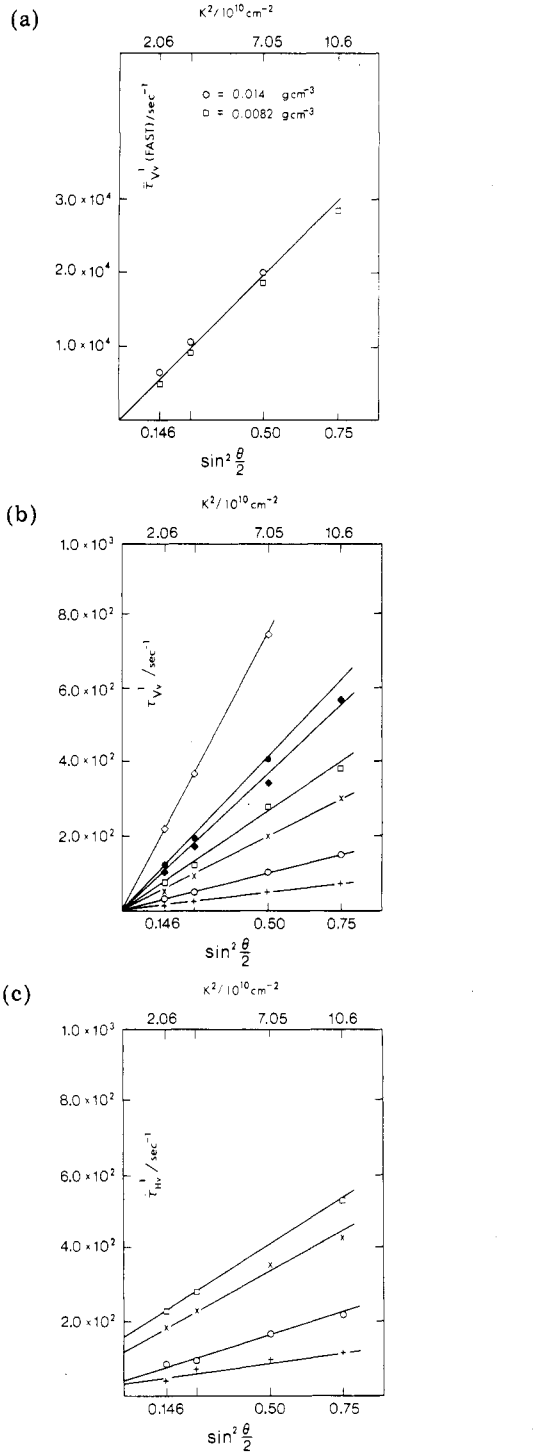

Figure 6. (a) $\bar{\tau}_{Vv}^{-1}(\text{fast})$ vs. $\sin^2(\theta/2)$ and K^2 for PBIC (molecular weight 7.5×10^4): (□) 0.0082; (○) 0.014 g cm^{-3}. (b) $\bar{\tau}_{Vv}^{-1}(\text{slow})$ vs. $\sin^2(\theta/2)$ and K^2 for PBIC (molecular weight 7.5×10^4): (+) 0.015; (○) 0.014; (×) 0.0096; (□) 0.0082; (♦) 0.0061; (●) 0.0055; (◇) 0.0031 g cm^{-3}. (c) $\bar{\tau}_{Hv}^{-1}$ vs. $\sin^2(\theta/2)$ and K^2 for PBIC (molecular weight 7.5×10^4): (+) 0.0115; (○) 0.014; (×) 0.0096; (□) 0.0082 g cm^{-3}.

time correlation function, $\bar{\Gamma}_{Vv}(\text{slow})$. Table II lists the cooperative translational diffusion coefficient, $D_{t\parallel}$, as a function of concentration. In Figure 7a, the cooperative translational diffusion coefficient is plotted against concentration. $D_{t\parallel}$ is about 2 orders of magnitude slower than the free translational diffusion coefficient $D_{t0\parallel}$. In order to test eq 8, $(D_{t0\parallel} - D_{t\parallel})/D_{t0\parallel}$ was plotted against $c^{3/2}$ (Figure 7b). According to the Edwards and Evans model (eq 8), $(D_{t0\parallel} - D_{t\parallel})/D_{t0\parallel}$ should approach a straight line with a slope proportional to $(dL^2)^{3/2}$. Figure 7b demonstrates

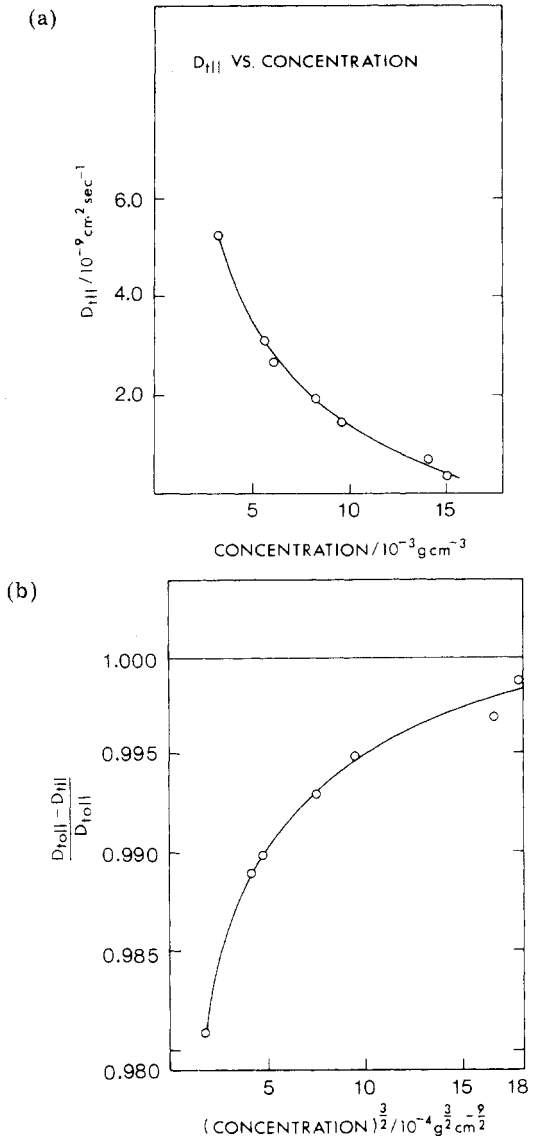

Figure 7. (a) Cooperative translational diffusion coefficient, $D_{t\|}$, vs. concentration for PBIC (molecular weight 7.5×10^4). (b) $(D_{t0\|} - D_{t\|})/D_{t0\|}$ vs. $c^{3/2}$ for PBIC (molecular weight 7.5×10^4). According to Edwards and Evans, this should approach a straight line with slope $\approx(dL^2)^{3/2}$.

Table II
Cooperative Translational and Rotational Diffusion Coefficients at Different Concentrations

c, g cm^{-3}	$10^9 D_{t\|}$,[a] cm^2 s^{-1}	D_r,[a] s^{-1}
0.0031	5.29	
0.0055	3.14	
0.0061	2.71	
0.0082	1.96	26.8
0.0096	1.46	20.0
0.014	0.72	7.38
0.015	0.32	5.93

[a] ±10%.

that $(D_{t0\|} - D_{t\|})/D_{t0\|}$ is not linear and the slope does not at all approach $(dL^2)^{3/2}$. It is reasonable to conclude, since the Edwards and Evans model predicts a free diffusion component and a cooperative diffusion component and since both have been observed, that the tube model with opening and closing gates is not at all unreasonable. In the presence of rod overlap, it should be noted that the cooperative translational diffusion coefficient ($D_{t\|}$) is like the slow mode in entangled polymer coils while the (fast) free translational diffusion component ($D_{t0\|}$) is related to

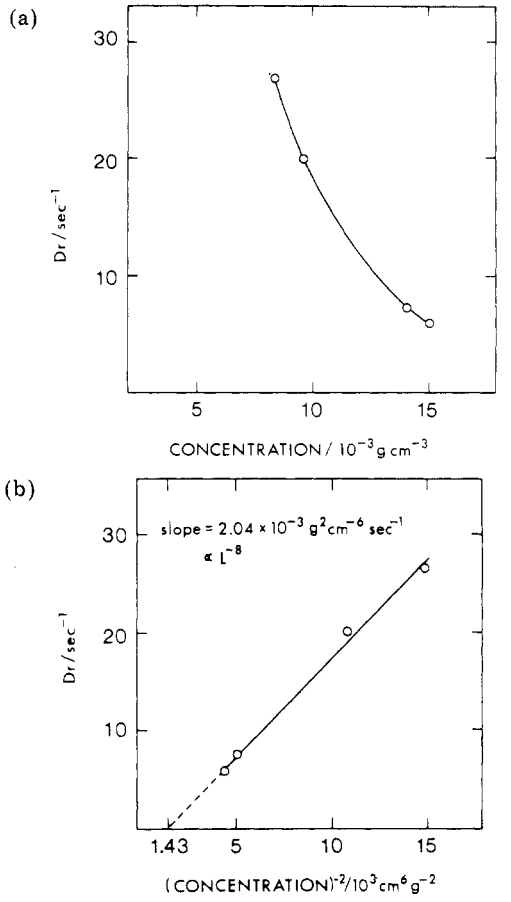

Figure 8. (a) Rotational diffusion coefficient, D_r, vs. concentration for PBIC (molecular weight 7.5×10^4). (b) Rotational diffusion coefficient, D_r, vs. (concentration)$^{-2}$ for PBIC (molecular weight 7.5×10^4). According to the Doi–Edwards theory of semidilute solutions, this should be a straight line with slope $D_{t0\|}L^{-8}$.

the motion of the rod between two gates in the Edwards tube. However, since the relationship of the cooperative translational diffusion coefficient with concentration (over a concentration range of 0.003 and 0.015 g/cm^3 with a computed $c^* \sim 0.01$ g/cm^3) does not follow the relationship given by Edwards and Evans, it is clear that the fine details of the model must be further explored. As the manner with which the average distance between two gates is determined is only approximate, the concentration dependence of the average distance between two gates in the Edwards tube is perhaps more complicated than Edwards and Evans suggest. In addition, the small amount of flexibility of the rod may have serious consequences on the size and even the shape of the Edwards tube. Polydispersity might have an added effect.

D_r as calculated from eq 39 is listed against concentration in Table II. In parts a and b of Figure 8, D_r is plotted against c and c^{-2}, respectively. According to the Doi and Edwards theory of the semidilute solution, $D_r/D_{t0\|}$ should be inversely proportional to c^2. The proportionality constant should be of order L^{-8}. If instead it is assumed that in semiconcentrate solution the cooperative translational motion, and not the free translational motion, determines the rotational motion, then $D_r/D_{t\|}$ should be inversely proportional to c^2 with a proportionality constant of L^{-8}. In other words

$$D_r \sim D_{t\|}(c^2L^8)^{-1} \tag{40}$$

instead of $D_r \sim D_{t0\|}(c^2L^8)^{-1}$ as predicted by eq 6. From Figure 8b it can be seen that D_r is proportional to c^{-2} and the proportionality constant is about equal to $L^{-8}/3$.

Therefore, $D_r/D_{t0\|} \sim c^{-2}L^{-9}$. By comparing Figures 8b and 7a, it is clear that $D_r/D_{t\|}$ is not proportional to c^{-2} at all. Therefore, for the concentrations studied, cooperative translational motions do not affect the rotational motion of the test rod while free translational motions are the dominant factor in determining the rotational motion, as shown in Figure 8b and eq 6 but not eq 40.

Conclusion

The time correlation function results indicate that the Edwards tube model is very useful in describing the motions of rods in solutions with concentrations on the order of $(dL^2)^{-1}$ (semiconcentrate region). Free translational motion persists in spite of the presence of other rods. Cooperative translational motion describes the effect of the presence of other rods and does have a strong concentration dependence. Rotational motion slows down with concentration. The concentration dependence of $D_{t\|}$ is not quite as expected even though polydispersity might be a contributing factor. It has been suggested that this is because the spacing of the gates within the tube is too approximate. On the other hand, the rotational diffusion coefficient does appear to follow the Doi and Edwards model for semidilute solution, suggesting that the rotation of a rod in semiconcentrate solution is dependent on the free translational motions of its neighboring rods (eq 6) and not on the cooperative translational motion (eq 40). In fact, we have observed

$$D_r \sim D_{t0\|}(c^2L^9)^{-1} \quad (41)$$

As we have demonstrated $D_r \propto c^{-2}$ in Figure 8b, $D_{t0\|}$ to be relatively independent of concentration in Figure 6a and $D_{t\|}$ to be concentration dependent in Figure 7a, we show $D_r/D_{t0\|} \propto c^{-2}$ while $D_r/D_{t\|} \not\propto c^{-2}$. It should be noted that the effect of rod thickness on rotation is independent of whether rotation is determined by cooperative translation or free translation. If rod thickness affects rotation, according to Doi,[26] $D_r \sim D_t(c^2L^9)^{-1}$ whereas if it does not $D_r \sim D_t(c^2L^8)^{-1}$. What we have observed is $D_t = D_{t0\|}$, demonstrating that the Edwards tube is still long in the concentration region of our investigation. From the values of D_r, $D_{t0\|}$, concentration, and rod length, we have estimated the L exponent to be 9 (as in eq 41) rather than 8 (as in eq 6). Therefore, although D_r depends on free diffusion, we cannot neglect the effects of rod thickness. In fact, rod thickness affects both translation and rotation, but cooperative translation does not affect rotation because of the length of the Edwards tube. It is interesting to note that Zero and Pecora[3] measured $D_r \propto L^{-9}$, yet they said they confirmed $D_r \propto L^{-8}$. Perhaps, they have confirmed Doi's original work instead of the Doi–Edwards model and showed the effects of rod thickness on rotation in semidilute solution.

Registry No. Poly(butyl isocyanate), 25067-04-3; PBIC, 26857-22-7.

References and Notes

(1) Berne, B. J.; Pecora, R. "Dynamic Light Scattering"; Wiley: New York, 1976; Chapter 7.
(2) Doi, M.; Edwards, S. F. *J. Chem. Soc., Faraday Trans. 2*, **1978**, *74*, 560.
(3) Zero, K. M.; Pecora, R. *Macromolecules* **1982**, *15*, 87.
(4) Jain, S.; Cohen, C. *Macromolecules* **1981**, *14*, 759.
(5) Edwards, S. F.; Evans, K. E. *J. Chem. Soc., Faraday Trans. 2*, **1982**, *78*, 113.
(6) Statman, D. E. Ph.D. Dissertation, State University of New York at Stony Brook, 1982.
(7) Tagami, Y. *J. Chem. Phys.* **1970**, *54*, 4990.
(8) Lehninger, A. "Biochemistry"; Worth: New York, 1976; Chapter 6.
(9) Maeda, T.; Fujime, S. *Macromolecules* **1981**, *14*, 809.
(10) Kubota, K.; Chu, B.; Fan, S.-F.; Dewey, M. M.; Brink, P.; Colflesh, D. E. *J. Mol. Biol.* **1983**, *166*, 329.
(11) Jamieson, A. M.; Southwick, J. G.; Blackwell, J. *J. Polym. Sci., Polym. Phys. Ed.* **1982**, *20*, 1513.
(12) Kubota, K.; Chu, B. *Biopolymers* **1983**, *16*, 105.
(13) Berry, G. C. *J. Polym. Sci., Polym. Symp.* **1978**, *No. 65*, 143.
(14) Wong, C.-P.; Ohnuma, H.; Berry, G. C. *J. Polym. Sci., Polym. Symp.* **1978**, *No. 65*, 173.
(15) Chu, S.-G.; Venkatraman, S.; Berry, G. C.; Einaga, Y. *Macromolecules* **1981**, *14*, 939.
(16) Kubota, K.; Chu, B. *Macromolecules* **1983**, *16*, 105.
(17) Aharoni, S. M. *Macromolecules* **1979**, *12*, 94.
(18) Bur, A. J.; Fetters, L. J. *Macromolecules* **1973**, *6*, 874.
(19) Ambler, M. R.; McIntyre, D.; Fetters, L. J. *Macromolecules* **1978**, *11*, 300.
(20) Bur, A. J.; Roberts, D. E. *J. Chem. Phys.* **1969**, *51*, 406.
(21) Kirkwood, K.; Auer, P. L. *J. Chem. Phys.* **1951**, *19*, 281.
(22) Fetters, L. J.; Yu, H. *Macromolecules* **1971**, *4*, 385.
(23) Shashoua, V. E.; Sweeney, W.; Tietz, R. F. *J. Am. Chem. Soc.* **1960**, *82*, 866.
(24) See, for example: Chen, F. C. Ph.D. Dissertation, State University of New York at Stony Brook, 1977.
(25) Koppel, D. E. *J. Chem. Phys.* **1972**, *57*, 4814.
(26) Doi, M. *J. Phys. (Paris)* **1975**, *36*, 607.

Dynamic Behavior of the Induced Polarization Arising from the Motion of Counterions Bound on a Rodlike Polyion

Akio Morita and Hiroshi Watanabe*

Department of Chemistry, College of Arts and Sciences, University of Tokyo, Komaba, Meguro-ku, Tokyo 153, Japan.

Received July 29, 1983

ABSTRACT: To elucidate the dynamic behavior of counterions moving on a polymer frame where polyions are located, the transient induced polarization due to the sudden removal of an applied electric field is calculated for four cases: (i) free motion of counterions on polyions, (ii) strongly bound counterions in a harmonic potential, (iii) motion of counterions due to the chemical reaction site model, and (iv) diffusion of counterions on sites resulting from a cosine potential. It is shown that (i), (ii), and (iii) lead to single-exponential decaying polarizations, while (iv) gives polarization mainly characterized by two relaxation times. The former cases are treated analytically, whereas the latter case is considered by carrying out numerical computations.

I. Introduction

Without directly involving a dynamical treatment, Mandel[1] considered the motion of counterions on a polyion based on a site model and estimated the relaxation time for the electric polarization. To overcome this difficulty, Oosawa[2] calculated the electric polarization, assuming that the fluctuation of counterions forms a mean field, which results in introducing a convolution integral in the Smoluchowski equation for the distribution of the counterions. Since this approach is based on thermodynamical concepts and is therefore phenomenological, it seems necessary for us to use a more explicit model with direct appeal to the

0024-9297/84/2217-1545$01.50/0